COMMUCATION

Fracture Behavior of Metallic Sodium and Implications for Battery Applications

Jungho Shin a and Matt Pharr*a

Received 00th January 20xx, Accepted 00th January 20xx

DOI: 10.1039/x0xx00000x

Sodium metal has emerged as a candidate anode material in rechargeable batteries owing to its high theoretical capacity, low standard reduction potential, and abundance in the earth's crust. Prior to practical deployment, it is critical to thoroughly assess sodium's mechanical properties, as to fully understand and thus help mitigate potential failure mechanisms. Herein, we examine the fracture behavior of sodium metal through tensile tests in an inert environment. We find that sodium is nearly insensitive to flaws (crack-like features), i.e., its effective strength is virtually unaffected by the presence of flaws. Instead, under tension, sodium exhibits extreme necking that leads to eventual failure. We also characterize the microstructural features associated with fracture of sodium through scanning electron microscopy studies, which demonstrate several features indicative of highly ductile fracture, including wavy slip and microvoid formation. Finally, we discuss the implications of these experimental observations in the context of battery applications.

Introduction

With increasing demands for mobile power, constructing better energy storage systems has become imperative. Numerous materials¹⁻⁴ have been studied to improve the capacity and cyclic performance of rechargeable batteries, and anodes based on alkali metals⁵⁻⁸ have gained traction as the next generation of rechargeable batteries. Indeed, sodium metal is theoretically the ideal candidate for anodes of Na-ion batteries, owing to its high theoretical capacity, comparably low standard reduction potential of -2.713 V, and relatively low price stemming from its wide availability in the earth's crust. Additionally, many materials can be alloyed with sodium, which is critical in developing optimized and sustainable energy storage systems9, ¹⁰. Still, prior to practical deployment, it is critical to assess the mechanical properties of sodium metal. Indeed, mechanical damage induced during electrochemical cycling has limited the commercialization of several high-capacity chemistries¹¹⁻¹⁴.

Electrochemical charging and discharging of battery electrodes can induce significant mechanical stresses¹⁵⁻¹⁷. During its lifetime under electrochemical cycling, an electrode material typically experiences both tensile and compressive stresses¹⁷⁻²⁴. For example, lithiation or sodiation of a host electrode usually causes the host material to expand, which generates a field of stress (often highly compressive) under constraint^{17, 19-21}. Delithiation or de-sodiation of that same host electrode usually causes the host material to shrink, which can produce the

opposite sign of stress (e.g., tension)^{17, 19-21}. Likewise, materials that readily plastically deform (sodium metal itself has a very low yield strength²⁵) have been shown to experience both tensile and compressive stresses at varying locations within their structure at any given point in time during the charge/discharge process^{20, 21, 26}. Kinetic limitations, e.g., fast charge/discharge relative to the time for diffusion of species (e.g., Li, Na) through the electrode exacerbate this scenario 18, 21, producing relatively large stresses in the electrode material. Similarly, electrochemical deposition (e.g., electroplating of Li/Na²⁷) and stripping can produce either tensile or compressive stresses in a given material, depending on details of the growth/deposition mechanism^{28, 29}. For instance, Wang et al. reported that tensile stresses are generated by the stripping process at a solid-state lithium-metal battery interface³⁰. Additionally, batteries are often placed under so-called stack pressures, which have been shown to significantly affect the electrochemical performance of several systems³¹⁻³³. For instance, Müller et al. reported that preapplied pressures change the ionic pore resistance, the charge transfer resistance, and reversibility of a Li-ion system with a graphite-based anode and a LiNi_{0.6}Mn_{0.2}Co_{0.2}O₂ cathode³². Likewise, Zhou et al. found that external pressure applied to a cell decreases the internal resistance and increases the lifetime in a lithium-ion pouch cell with a graphite-based anode and a LiNi_xCo_yMn_zO₂ cathode³⁴. Overall, significant tensile stresses can be generated during electrochemical cycling, which can lead to fracture of the active materials, as has been demonstrated in several battery systems^{17, 19, 35-38}. This mechanical damage can lead to eventual failure of not only the battery electrode itself but also of the entire electronic device, for example by inducing short circuits which can induce fire hazards.

^a· Department of Mechanical Engineering, Texas A&M University, College Station, TX, 77840, USA. E-mail: m-pharr@tamu.edu Electronic Supplementary Information (ESI) available: [details of any supplementa]

Electronic Supplementary Information (ESI) available: [details of any supplementary information available should be included here]. See DOI: 10.1039/x0xx00000x

As such, particularly with the emergence of all-solid-state systems, it is important to fully characterize the mechanical

properties of each component prior to practical deployment. Indeed, recent work has developed a solid-state battery using sodium metal as the anode, which has demonstrated the advantages of sodium in reducing the contact resistance with the solid electrolyte due to the soft, liquid-like characteristics of sodium, even as compared to metallic lithium³⁹. However, largely due to sodium's reactivity in air, studies on mechanical properties of Na metal are relatively limited^{25, 40-45}, and many unanswered questions remain. For example, what mechanisms are associated with crack formation and propagation in sodium? How sensitive is sodium to the presence of flaws? How do volume changes induced by sodiation/de-sodiation affect electrochemical performance? What mechanisms and conditions lead to dendrite formation and contact losses with solid electrolytes? To fully understand and provide insight and thus solutions to these issues, it is critical to fully characterize and analyze the mechanical behavior of sodium metal under various conditions and geometries.

A few studies have investigated the mechanical properties of sodium metal. Recently, Fincher et al. conducted nanoindentation and bulk compression tests of sodium metal 25 . Their nanoindentation studies found the elastic modulus of polycrystalline sodium metal to be 3.9 ± 0.5 GPa. They discovered that the nanoindentation hardness of Na metal decreases with indentation depth, i.e., Na exhibits an indentation size effect, which hinted at a material size effect in sodium. The authors also found that sodium metal exhibits highly strain-rate sensitive and creep-prone behavior. In another study, Wang et al. reported the yield strength of sodium metal as 0.19 - 0.28 MPa under tension and compression, and also found the elastic, shear, and bulk moduli to be 4.6, 1.7, and 8.5 GPa, respectively, using

acoustic techniques⁴⁰. However, the fracture behavior of sodium metal remains unstudied, including its sensitivity to the presence of flaws as well as the microstructural features and phenomena associated with fracture and damage. Since fracture of an electrode has a fatal effect on the cyclic performance of a battery, it is critical to understand the precise mechanisms of formation and growth of cracks and the corresponding ramifications in terms of battery performance.

In this paper, we examine the fracture behavior of Na metal through tensile tests in an inert environment, as to assess the sensitivity of Na to the presence of crack-like flaws. We further characterize the macroscopic and microstructural features associated with fracture of Na through real-time optical imaging and scanning electron microscopy. In addition, we report the stress-strain and corresponding fracture behavior of sodium at different strain rates. We conclude by discussing the implications of these experimental observations in the context of battery applications.

Experimental Section

Sodium sample preparation

All sample preparation was carried out in argon-filled glovebox with less than 0.1 ppm O_2 and moisture (H₂O) levels. Sodium

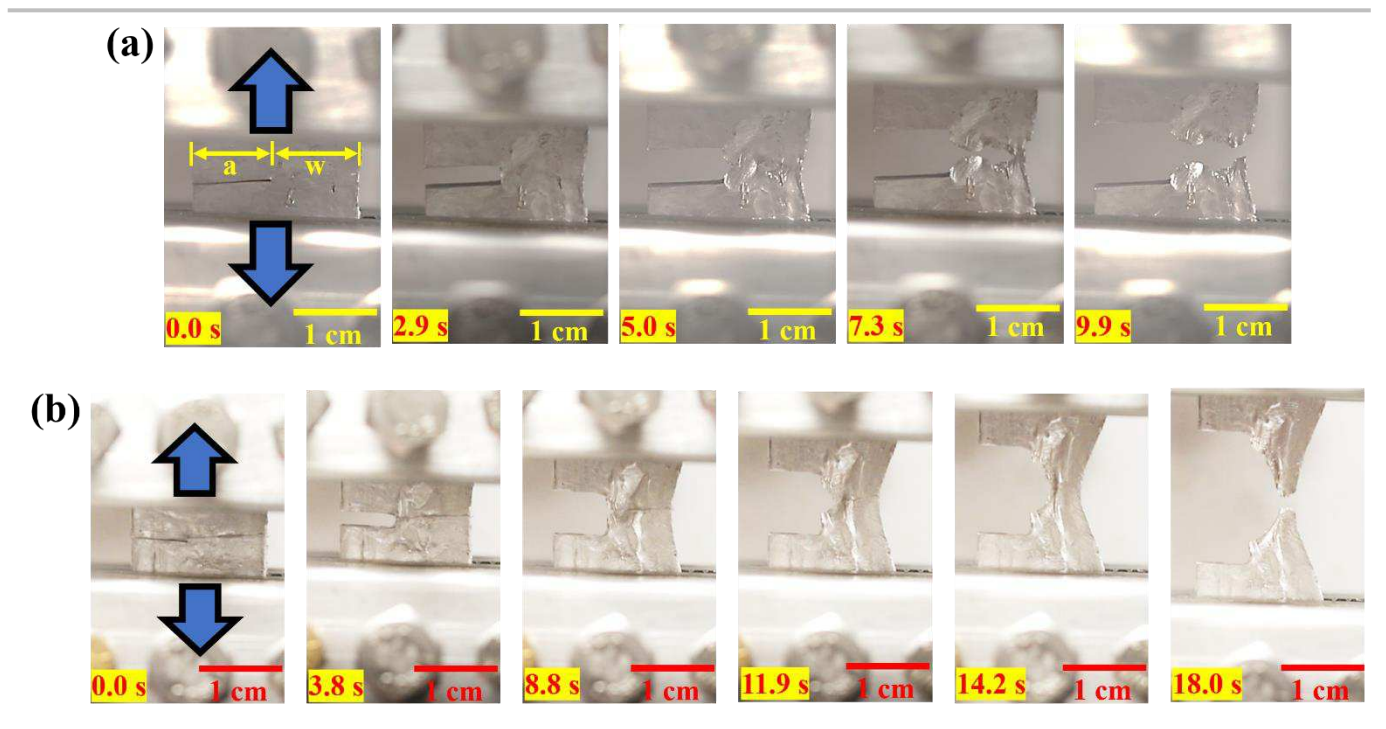


Fig. 1 Photographs of tensile testing of Na metal in a glovebox. (a) and (b) show two samples with varying levels of strain prior to complete fracture.

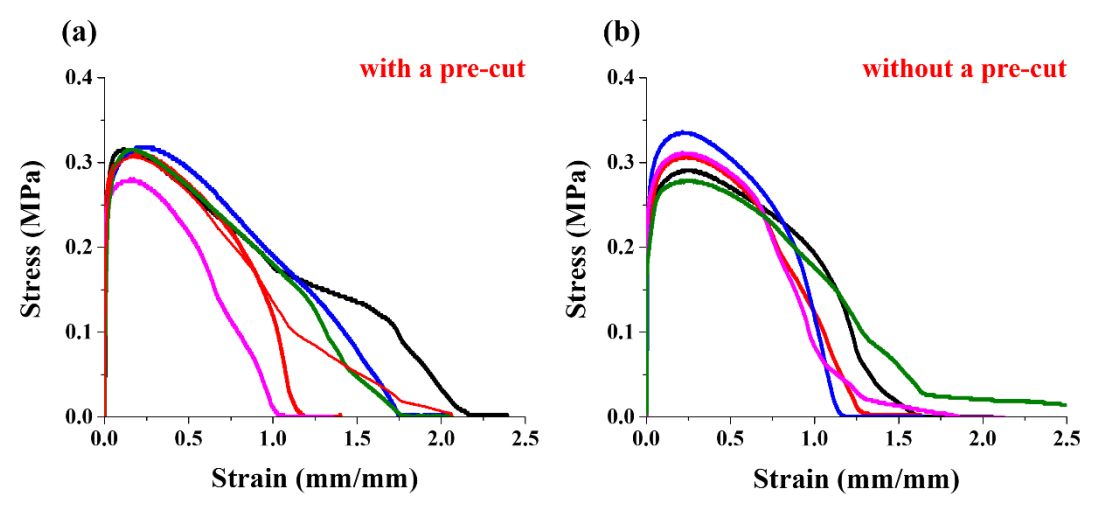


Fig. 2 Engineering stress-strain relationships from uniaxial tension testing of Na metal at a strain rate of 0.1 s⁻¹ for specimens (a) with a precut and (b) without a pre-cut. Multiple replicates are indicated by different colored curves.

sticks (coated in film of protective hydrocarbon oil, $\geq 98.5\%$ purity, $1 \times 1 \times 7$ inch) were purchased from Alfa Aesar (Stock No. L13285-24). We then manually removed the oxidized layers and thinned the specimens with a rolling pin to a thickness of approximately 3 mm. Thicknesses were measured with Vernier calipers at three points on each sample, and an average was taken. Specimens were then cut into a section approximately 2 cm wide and 3 cm long and stored in mineral oil before tensile testing. Vaseline petroleum jelly was administered to the sodium to further protect the sample surface from undesirable chemical reactions during tensile testing.

Tensile testing

Tensile testing utilized a custom-built tensile tester in a glove box maintained in an argon environment to prevent undesirable chemical reactions. One arm of the tensile tester contains a load cell (LC703-200, Omega Engineering) that measures the load as a function of time through an INF-USB2 model data acquisition system (Interface Inc.) in conjunction with a ClearPath-MCPV model integrated servo motor system (Teknic) assembled onto an FGS-250W test stand (SHIMPO). Load cell calibration was validated against a 1 kN load cell of an Instron 5943 benchtop tensile tester.

In pre-cut specimens, a cut was made with a fresh razor blade at the edge of the specimen with a length of approximately 7-10 mm. The sample was firmly fixed to the tensile test using screwbased grips with an initial distance between the grips of 1 cm, and the load data was measured at 100 Hz. The strain rate was 0.1 s⁻¹ (1 mm/s) for the majority of the tests and also at 0.01 s⁻¹ (0.1 mm/s) for the "slow tests" to study rate effects. After tensile testing, several samples were examined post-mortem to investigate microstructural details of the fractured surfaces. Specimens were immediately placed in a hermetic vacuum transfer vessel (VWR® Desi-VacTM Container) after removing from the glove box. The samples were then quickly loaded into an SEM chamber (Tescan FERA-3 Model GMH Focused Ion

Beam Microscope) for microscopy studies. All tensile testing and SEM data was collected within 6 hours of sample preparation.

Results and Discussion

Fig. 1 shows a time-sequence during tensile testing of Na metal in a glovebox. In several samples, a pre-cut (of length α as shown in Fig. 1(a)) was introduced into the sample to assess the sensitivity of Na to the presence of a flaw. During loading, all samples yielded globally relatively quickly, followed by substantial plastic deformation. Likewise, due to the extreme ductility of Na, the crack-tip blunted substantially prior to crack growth (Fig. 1 and Videos S1 and S2). The crack grew relatively slowly, i.e., not "immediately" or "catastrophically", in a tortuous path, prior to complete failure, as shown in Fig. 1 and Videos S1 and S2. These images and videos reveal that Na is extremely soft and exhibits significant plastic deformation prior to crack propagation, as well as during crack growth. We also performed the same test protocol in specimens without a pre-cut to quantify how a flaw affects the effective strength of Na.

Fig. 2 presents engineering stress-strain curves from tensile testing of Na metal. To determine the engineering stress from the measured load, the cross-sectional area was defined as the product of the width and thickness of the sample for the specimens without a pre-cut. For the specimens with a pre-cut, the cross-sectional area was taken as the product of the thickness and the un-cracked width (labeled "w" in Fig. 1). Previous studies have shown that the hardness of a metal from an indentation test correlates well with the flow stress from a uniaxial test at a strain of ≅0.08 from the uniaxial test ⁴⁶. As such,

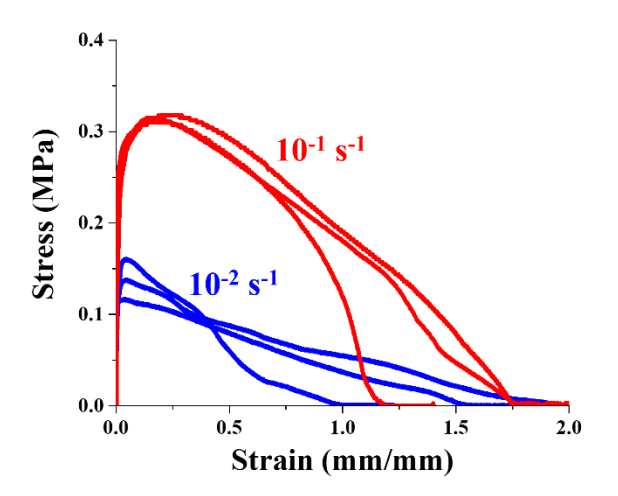


Fig. 3 Engineering stress-strain relationships from uniaxial tension testing of pre-cut specimens of Na metal at varying strain rates of 0.01 s^{-1} (blue) and 0.1 s^{-1} (red).

herein we report the flow stress at a strain of 0.08, e.g., as to compare with existing studies from nanoindentation. At strains of 0.08 and at an applied nominal strain rate of 0.1 s⁻¹, the flow stress of the specimens with a pre-cut was 0.29 ± 0.03 MPa (mean \pm standard deviation), and the flow stress of specimens without a pre-cut was 0.29 ± 0.04 MPa. These experiments indicate that the effective strength of Na is essentially insensitive to the presence of a flaw. Likewise, although we observe a large variability in the strain at ultimate failure from sample to sample

(likely due to the stochastic nature of the crack path during propagation observed in these specimens), we do not observe any obvious differences in the strain at ultimate failure between the specimens with a pre-cut as compared to the specimens without a pre-cut. As such, Fig. 2 provides clear direct evidence that the presence of a flaw (pre-cut) does not affect the mechanical behavior of sodium metal, beyond the simple reduction in cross-sectional area that it induces.

With an eye toward mechanical modeling, herein we provide a simple scaling analysis from a fracture mechanics perspective in light of these experimental results. To utilize linear elastic fracture mechanics (LEFM), the size of the plastic zone near the crack tip should be much smaller than the overall dimensions of the specimen (as well as the crack length itself). The plastic zone size, r_p , near a crack-tip is given by $r_p = (1/2\pi)(K_{IC}/\sigma_Y)^2$, where $\sigma_{\rm Y} = 0.29$ MPa from our experimental measurements⁴⁷. Although the fracture toughness of sodium has not been measured, even if we use an over-conservatively low value of $K_{IC} = 1MPa\sqrt{m}$, the plastic zone size is estimated as 1.9 meters! This simple scaling analysis demonstrates that fracture of sodium will never meet the small-scale yielding condition under any practical conditions, and thus LEFM does not provide any real utility in terms of modeling the behavior of sodium metal. Instead, as shown in Fig. 2, sodium metal is almost completely insensitive to the presence of the flaw, i.e., in terms of its influence on the stress/strain that it can withstand prior to failure.

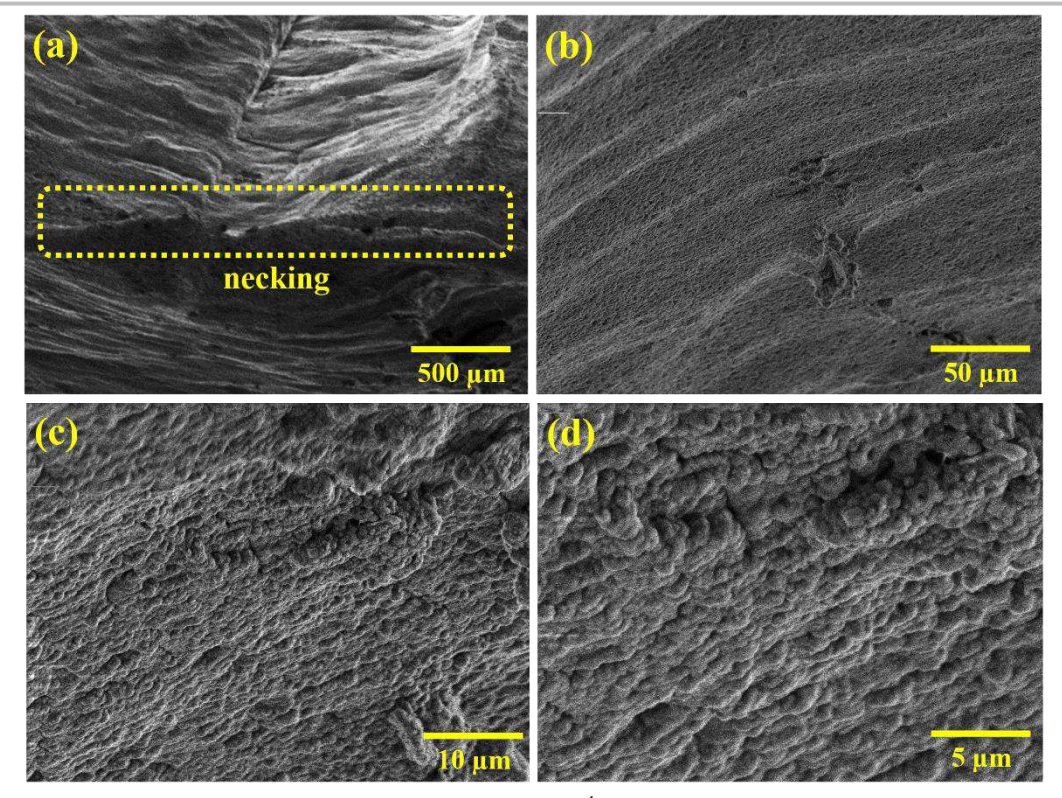


Fig. 4 SEM images of a fractured surface of Na tested at a strain rate of 0.1 s^{-1} . (a) is a zoomed-out image that shows evidence of wavy slip and that extreme necking occurs through the thickness of the specimen, nearly down to a single line. (b) is a zoomed-in image showing further details of the observed wavy slip. (c) and (d) are further zoomed-in images that show rough surfaces indicative of microvoid formation.

Fig. 3 displays several engineering stress-strain curves under tension in pre-cut sodium samples at two different strain-rates of $10^{-1}~\rm s^{-1}$ and $10^{-2}~\rm s^{-1}$. The measured flow stresses at strains of 0.08 are 0.29 ± 0.03 MPa at a strain rate of $10^{-1}~\rm s^{-1}$ and 0.15 ± 0.03 MPa at a strain rate of $10^{-2}~\rm s^{-1}$. Indeed, sodium exhibits a marked strain-rate sensitivity, owing to its relatively low melting point (98°C) and correspondingly high homologous temperature (T/T_m = 0.8 at room temperature). This strain-rate dependent stress response is in good agreement of previous studies on Na by Fincher et al.²⁵ under compression and Wang et al.⁴⁰ under tension.

To aid in understanding the microstructural mechanisms that lead to the observed mechanical behavior of Na, we performed SEM studies of the fractured surfaces, as shown in Fig. 4 and 5. To do so, samples were transferred in a hermetic container from the glovebox to the SEM chamber with only a few seconds of air exposure during transfer. Petroleum jelly was also applied to the surface of the sample to further mitigate chemical reactions with ambient air.

Fig. 4(a) shows that extremely ductile necking occurred through the thickness of the specimen, almost down to a single line along its width (as shown from left to right near the middle of Fig. 4(a)). Additionally, the fractured surfaces appear striated (interestingly as is often seen in fatigue), and evidence of wavy slip during the fracture process is evident, as in Fig. 4(b). In terms of the potential origin of this latter observation, sodium has a body-centered cubic (BCC) structure at room temperature. The

slip system that is most commonly activated in BCC materials is the $\{110\}\langle \bar{1}11\rangle$ system. The $\{110\}$ planes are stacked in an ABABAB sequence, and screw dislocations can move in any direction on these {110} planes⁴⁸, which is conducive to wavy slip⁴⁹. Also, since the BCC structure is not close-packed, nonplanarity of screw dislocations occurs more easily^{50, 51}. Likewise, the melting point of sodium is around 98°C, i.e., at room temperature the homologous temperature of sodium is around T/T_m = 0.8. At higher homologous temperatures, thermally-activated screw dislocations can more easily move in the {110}planes⁵². Additionally, at higher homologous temperatures, dislocation movement is not confined to single slip plane because cross-slip and dislocation climb can readily occur, which is also conducive to the formation of wavy-type slip. However, we should be clear that our observations of what appears to be wavy slip does not necessarily imply that wavy slip is the dominant deformation mechanism in Na metal. Related to this point, Na has a high homologous temperature even at room temperature, which implies that specific creep-based mechanisms are likely important in sodium's deformation mechanics. Determining the precise dominant deformation mechanism requires more detailed microstructural studies than we have performed herein and is an interesting area for future work. Fig. 4(c) and 4(d) show clear evidence of rough, dimpled features on the fractured surface of Na, which is typical of ductile materials. As such, we surmise that the observed ductile fracture of sodium originates from the formation of microvoids. As plastic deformation proceeds, the microvoids form and coalesce, eventually leading to macroscopic failure.

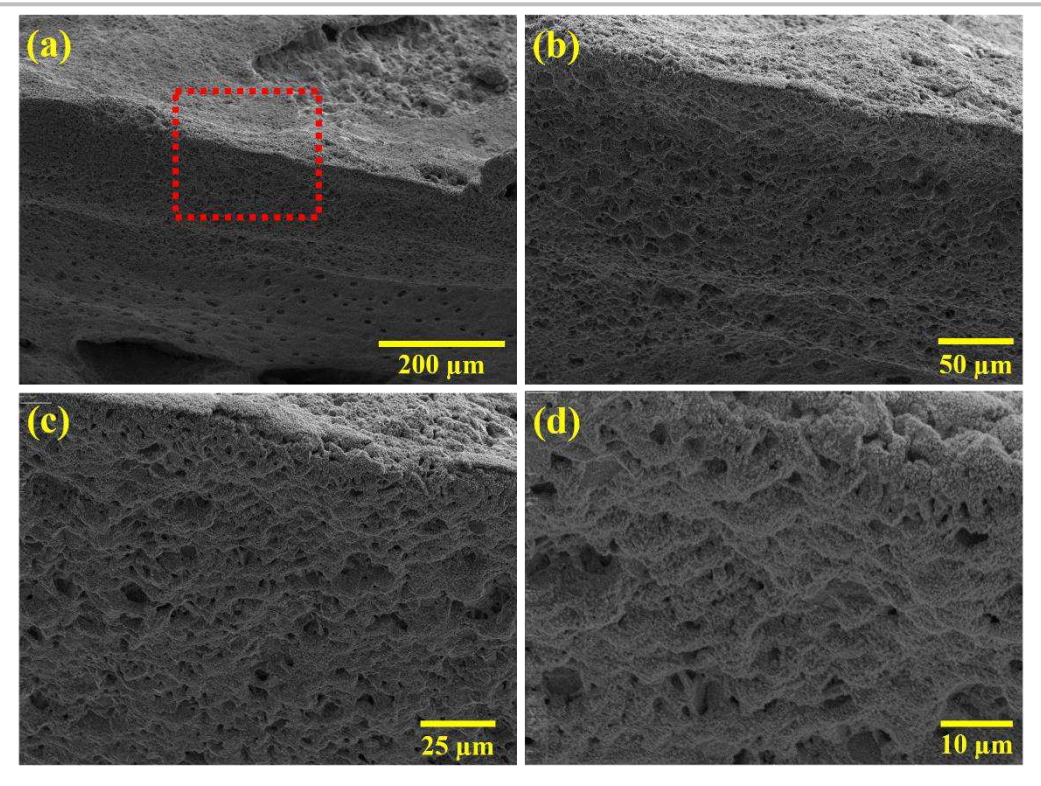


Fig. 5 SEM images of a fractured surface of Na tested at lower strain rate of 0.01 s^{-1} . (a) is a zoomed-out image showing that extreme necking occurs through the thickness of the specimen, almost down to a single line. (b) is a zoomed-in image of the red dotted box in (a). (c) and (d) are further zoomed-in images that show further details of the rough surfaces indicative of microvoid formation.

Fig. 5 shows SEM images of a fractured surface of Na when tested at a lower strain rate of 10^{-2} s⁻¹. Although we observed significantly lower flow stress at this lower strain rate (Fig. 3), we did not observe any obvious qualitative differences in the fracture surface relative to that at the higher strain rate. Namely, the fractured surface at this lower strain rate still shows rough, dimpled features indicative of microvoid formation during fracture.

Implications for Na metal batteries

Sodium metal batteries are desirable in terms of their high theoretical capacity, comparably low standard reduction potential of -2.713 V, and relative abundance in the earth's crust^{53, 54}. However, undesirable dendrite formation often occurs during electrochemical cycling, which is accompanied by risks such as short circuits, reduced capacity, and safety issues (fire hazards). Since sodium is extremely reactive and has low flow stress, relatively large flaws can form during the fabrication process as well as during electrochemical cycling. However, as shown in Fig. 2, sodium demonstrates remarkably similar mechanical behavior regardless of the presence of flaws. Here, centimeter-scale cracks were used for the experiment, in line with the dimensions of the tested samples. However, in real battery applications, the flaws will be much smaller, e.g., flaws manufacturing processes sodium cycling/plating/deposition typically exist in the micron or submicron length scale. Indeed, one set of our studies here involves specimens without a pre-cut, which presumably have small defects in them from the manufacturing process (e.g., microcracks). We then compare this set of samples to another set with large (mm to cm-scale) flaws. Even in this extreme example in going from very small defects that are undetectable (at least by our eyes) to specimens with very large cracks (mm to cm-scale), we observe essentially no sensitivity of the mechanical response to the presence of these flaws. Extending this logic, our results also suggest (albeit it indirectly) that micro-scale cracks will very likely have similar mechanical characteristics (e.g., flaw insensitivity) to our experimental tests performed here at larger scale. This feature is desirable from the perspective of predicting its mechanical behavior reliably, even under different fabrication and operation conditions. Likewise, this property of sodium is desirable from a failure/damage perspective in that the presence of flaws does not reduce its effective strength, as is the case in most engineered systems.

Barai et al.⁵⁵ reported that lithium dendrites can be suppressed by external pressures. It is likely that a similar tactic can be employed in sodium-based batteries, given sodium's similarities to lithium in terms of mechanical properties and charging/discharging through an alloying/de-alloying process. To first order, when a dendrite forms, its flow stress must exceed the external pressure to allow it to grow. The dendrite can grow until its flow stress equilibrates with the external pressure, above which it plastically deforms and expands in-plane^{56, 57}. Our results provide values of the flow stress of Na metal, which could

be used in guidelines in suppressing dendrite formation. We report a flow stress of about 0.29 ± 0.03 MPa at strain rate of 0.1 s⁻¹ and 0.15 ± 0.02 MPa at strain rate of 0.01 s⁻¹, which is comparable to reported values in literature of 0.19-0.28 MPa under tension/compression from Wang et al.⁴⁰ and 0.10-0.25 MPa at strain rates between 10^{-4} and 10^{-2} s⁻¹ under compression from Fincher et al²⁵. These values are smaller than the reported yield strength of approximately 0.57-1.26 MPa for lithium metal⁵⁸, which is likely an advantage for sodium in more readily inhibiting dendrite growth and thus in preventing short circuits in sodium metal-based solid-state batteries, as has been discussed in detail in previous work^{25, 39}.

In terms of dendrite formation, which is one of the most important issues in alkali metal-based batteries, representative sizes are typically in the nanometer scale (e.g., hundreds of nanometers). Liu et al. reports that the yield strength of nanostructured Na is much higher than that of bulk Na⁴¹. Likewise, Fincher et al. studied the mechanical properties of Na at small scale (down to hundreds of nm), and reported that sodium exhibits a significant size effect at room temperature²⁵. Namely, through nanoindentation methods, they found that sodium becomes softer as the indent depth is larger, i.e., sodium is stronger/harder at smaller length scales. Here, we have found that sodium is nearly insensitive to the presence of even large flaws. As such we expect that this observation extends down to very small length scales. In other words, from these studies, we predict that dendrites will likewise be unaffected by the presence of flaws, at least in the fracture mechanics sense of flaw sensitivity and its effect on overall mechanical behavior.

In addition, the soft nature of Na metal will likely enhance its interfacial contact with a solid electrolyte in solid-state batteries, thereby increasing stability, cycle life, and critical current densities. Namely, in solid-state batteries, internal circuits are often disconnected by external forces, temperature changes, etc., which can lead to the formation of gaps between components (e.g., between a metal anode and a solid electrolyte). However, sodium's facile flow renders it conducive to filling in voids that often form, thereby maintaining the internal connection and reducing interfacial resistance. Moreover, recent research has studied electrodes that implement multiple phases of active materials. It has been found that metallic Na and Na-alloy based electrodes can readily flow plastically, thus improving interfacial contact and thereby increasing critical current densities that can be sustained prior to degradation³⁹.

Furthermore, the relatively low flow stress, large ductility, and flaw insensitivity of Na metal are conducive to applications in flexible batteries⁵⁹⁻⁶¹. Specifically, flexible batteries must be readily deformable (compliant/soft) and must remain mechanical robust during repeated loading. Due to its relatively low flow stress and large ductility, sodium metal indeed has the requisite flexibility for users to freely change its shape as desired, thus providing tremendous promise in developing flexible batteries. Moreover, Na metal is highly insensitive to the presence of

flaws, which could aid in maintaining its mechanical properties after repeated loading.

Conclusions

In this work, we have characterized the fracture behavior of Na metal. The stress-strain curves of specimens with and without pre-cuts (crack-like flaws) were remarkably similar, thereby indicating that sodium is nearly insensitive to the presence of flaws, owing to its extreme ductility. Instead, under tension, Na exhibited through-thickness necking down to nearly a line that led to eventual failure at large macroscopic strains. This flaw insensitivity is desirable from the perspective of predicting Na's mechanical behavior reliably, even under different fabrication and operating conditions. Likewise, sodium's flaw insensitivity is desirable from a failure/damage perspective in that the presence of flaws will not reduce its effective strength, which contrasts with most engineered systems. We also characterized the microstructural features associated with fracture of Na through scanning electron microscopy. These studies revealed several features indicative of highly ductile fracture, including wavy slip and microvoids. Overall, this study has provided fundamental insight into damage and fracture of Na metal, which can aid in designing Na-based architectures and corresponding charging conditions that avert mechanical damage.

Author Contributions

Jungho Shin: Conceptualization, Software, Validation, Formal analysis, Investigation, Data Curation, Writing - Original Draft

Matt Pharr: Conceptualization, Writing - Review & Editing, Supervision, Project administration, Funding acquisition

Conflicts of interest

There are no conflicts to declare.

Acknowledgements

We acknowledge the support of the National Science Foundation under award number DMR-1944674. We would also like to acknowledge the Texas A and M University Materials Characterization Core Facility (RRID:SCR_022202).

References

- 1. Y. Zhang, Y. Luo, C. Fincher, S. McProuty, G. Swenson, S. Banerjee and M. Pharr, *Energy Storage Materials*, 2019, **16**, 491-497.
- Z. Guo, C. Li, J. Liu, Y. Wang and Y. Xia, Angewandte Chemie, 2017, 129, 7613-7617.
- 3. R. Pfenninger, M. Struzik, I. Garbayo, E. Stilp and J. L. Rupp, *Nature Energy*, 2019, **4**, 475-483.

- Y. Zhang, X. Xia, B. Liu, S. Deng, D. Xie, Q. Liu, Y. Wang, J. Wu, X. Wang and J. Tu, *Advanced Energy Materials*, 2019, **9**, 1803342.
- 5. J. Xiang, L. Yang, L. Yuan, K. Yuan, Y. Zhang, Y. Huang, J. Lin, F. Pan and Y. Huang, *Joule*, 2019, **3**, 2334-2363.
- W. Tang, X. Yin, S. Kang, Z. Chen, B. Tian, S. L. Teo, X. Wang, X. Chi, K. P. Loh and H. W. Lee, *Advanced Materials*, 2018, 30, 1801745.
- Z. W. Seh, J. Sun, Y. Sun and Y. Cui, ACS central science, 2015, 1, 449-455.
- 8. P. Hundekar, S. Basu, X. Fan, L. Li, A. Yoshimura, T. Gupta, V. Sarbada, A. Lakhnot, R. Jain and S. Narayanan, *Proceedings of the National Academy of Sciences*, 2020, **117**, 5588-5594.
- X. Zheng, C. Bommier, W. Luo, L. Jiang, Y. Hao and Y. Huang, *Energy Storage Materials*, 2019, 16, 6-23.
- 10. J. Qian, Y. Chen, L. Wu, Y. Cao, X. Ai and H. Yang, *Chemical Communications*, 2012, **48**, 7070-7072.
- Y. Zhang, Y. Luo, C. Fincher, S. Banerjee and M. Pharr, Journal of Materials Chemistry A, 2019, 7, 23922-23930.
- X. Zhu, Y. Xie, H. Chen and W. Luan, *International Journal of Fatigue*, 2021, 142, 105915.
- V. A. Sethuraman, N. Van Winkle, D. P. Abraham, A. F. Bower and P. R. Guduru, *Journal of Power Sources*, 2012, 206, 334-342.
- 14. K. An, P. Barai, K. Smith and P. P. Mukherjee, *Journal of the electrochemical society*, 2014, **161**, A1058.
- 15. T. E. Chin, U. Rhyner, Y. Koyama, S. R. Hall and Y.-M. Chiang, Electrochemical and solid-state letters, 2006, 9, A134.
- 16. M. Pharr, K. Zhao, X. Wang, Z. Suo and J. J. Vlassak, *Nano letters*, 2012, **12**, 5039-5047.
- M. Pharr, Y. S. Choi, D. Lee, K. H. Oh and J. J. Vlassak, *Journal of Power Sources*, 2016, 304, 164-169.
- M. Pharr, Z. Suo and J. J. Vlassak, *Journal of Power Sources*, 2014, **270**, 569-575.
- M. Pharr, Z. Suo and J. J. Vlassak, *Nano letters*, 2013, 13, 5570-5577.
- 20. K. Zhao, M. Pharr, J. J. Vlassak and Z. Suo, Journal, 2011.
- 21. K. Zhao, M. Pharr, S. Cai, J. J. Vlassak and Z. Suo, *Journal of the American Ceramic Society*, 2011, **94**, s226-s235.
- S. Huang, F. Fan, J. Li, S. Zhang and T. Zhu, Acta materialia, 2013, 61, 4354-4364.
- P. Liu, N. Sridhar and Y.-W. Zhang, Journal of Applied Physics, 2012, 112, 093507.
- 24. Y. Lu and Y. Ni, Mechanics of Materials, 2015, **91**, 372-381.
- C. D. Fincher, Y. Zhang, G. M. Pharr and M. Pharr, ACS Applied Energy Materials, 2020, 3, 1759-1767.
- K. Zhao, M. Pharr, Q. Wan, W. L. Wang, E. Kaxiras, J. J. Vlassak and Z. Suo, *Journal of The Electrochemical Society*, 2011, 159, A238.
- 27. J. H. Cho, X. Xiao, K. Guo, Y. Liu, H. Gao and B. W. Sheldon, Energy Storage Materials, 2020, **24**, 281-290.
- 28. J. H. Cho, K. Kim, S. Chakravarthy, X. Xiao, J. L. Rupp and B. W. Sheldon, *Advanced Energy Materials*, 2022, 2200369.
- X. Zhang, Q. Xiang, S. Tang, A. Wang, X. Liu and J. Luo, *Nano Letters*, 2020, 20, 2871-2878.
- Z. Wang, X. Li, Y. Chen, K. Pei, Y.-W. Mai, S. Zhang and J. Li, Chem, 2020, 6, 2878-2892.
- A. Tang, J. Bao and M. Skyllas-Kazacos, Journal of power sources, 2014, 248, 154-162.

- V. Müller, R.-G. Scurtu, M. Memm, M. A. Danzer and M. Wohlfahrt-Mehrens, *Journal of Power Sources*, 2019, 440, 227148.
- 33. H. Luo, Y. Xia and Q. Zhou, *Journal of Power Sources*, 2017, **357**, 61-70.
- L. Zhou, L. Xing, Y. Zheng, X. Lai, J. Su, C. Deng and T. Sun, International Journal of Energy Research, 2020, 44, 6778-6791.
- H. Wang, Y. I. Jang, B. Huang, D. R. Sadoway and Y. M. Chiang, Journal of the Electrochemical Society, 1999, 146, 473.
- 36. M. G. Lazarraga, S. Mandal, J. Ibanez, J. M. Amarilla and J. M. Rojo, *Journal of power sources*, 2003, **115**, 315-322.
- D. Wang, X. Wu, Z. Wang and L. Chen, *Journal of Power Sources*, 2005, **140**, 125-128.
- 38. H. Gabrisch, J. Wilcox and M. Doeff, *Electrochemical and Solid-State Letters*, 2008, **11**, A25.
- R. J.-Y. Park, C. M. Eschler, C. D. Fincher, A. F. Badel, P. Guan, M. Pharr, B. W. Sheldon, W. C. Carter, V. Viswanathan and Y.-M. Chiang, *Nature Energy*, 2021, 6, 314-322.
- 40. M. J. Wang, J.-Y. Chang, J. B. Wolfenstine and J. Sakamoto, *Materialia*, 2020, **12**, 100792.
- Q. Liu, L. Zhang, H. Sun, L. Geng, Y. Li, Y. Tang, P. Jia, Z. Wang, Q. Dai and T. Shen, ACS Energy Letters, 2020, 5, 2546-2559.
- 42. S. Quimby and S. Siegel, *Physical Review*, 1938, **54**, 293.
- 43. W. B. Daniels, *Physical Review*, 1960, **119**, 1246.
- 44. M. E. Diederich and J. Trivisonno, *Journal of Physics and Chemistry of Solids*, 1966, **27**, 637-642.
- 45. R. Martinson, *Physical Review*, 1969, **178**, 902.
- 46. D. Tabor, *The hardness of metals*, Oxford university press, 2000.
- 47. L. Barker and F. Baratta, *Journal of Testing and Evaluation*, 1980, **8**, 97-102.
- 48. R. E. Smallman and R. J. Bishop, *Modern physical metallurgy and materials engineering*, Butterworth-Heinemann, 1999.
- 49. M. Sarvghad, T. Chenu and G. Will, *Corrosion Science*, 2017, **116**, 88-97.
- X. Hu and S. Wang, *Philosophical Magazine*, 2018, **98**, 484 516.
- 51. B. Chen, S. Li, H. Zong, X. Ding, J. Sun and E. Ma, *Proceedings of the National Academy of Sciences*, 2020, **117**, 16199-16206.
- 52. G. Kostorz, H. Calderon and J. Martin, Fundamental Aspects of Dislocation Interactions: Low-Energy Dislocation Structures III, Elsevier, 2013.
- 53. L. Ye, M. Liao, T. Zhao, H. Sun, Y. Zhao, X. Sun, B. Wang and H. Peng, *Angewandte Chemie*, 2019, **131**, 17210-17216.
- M. Zhu, G. Wang, X. Liu, B. Guo, G. Xu, Z. Huang, M. Wu, H.
 K. Liu, S. X. Dou and C. Wu, *Angewandte Chemie*, 2020, 132, 6658-6662.
- 55. P. Barai, K. Higa and V. Srinivasan, *Journal of The Electrochemical Society*, 2018, **165**, A2654.
- 56. X. Shen, R. Zhang, P. Shi, X. Chen and Q. Zhang, *Advanced Energy Materials*, 2021, **11**, 2003416.
- X. Zhang, Q. J. Wang, K. L. Harrison, K. Jungjohann, B. L. Boyce, S. A. Roberts, P. M. Attia and S. J. Harris, *Journal of The Electrochemical Society*, 2019, 166, A3639.
- C. D. Fincher, D. Ojeda, Y. Zhang, G. M. Pharr and M. Pharr, *Acta Materialia*, 2020, **186**, 215-222.

- J. Ma, S. Zheng, P. Das, P. Lu, Y. Yu and Z.-S. Wu, Small Structures, 2020, 1, 2000053.
- 60. T. Liu, X. Y. Yang and X. B. Zhang, Advanced Materials Technologies, 2020, 5, 2000476.
- T. Liu, X. I. Feng, X. Jin, M. z. Shao, Y. t. Su, Y. Zhang and X.
 b. Zhang, Angewandte Chemie, 2019, 131, 18408-18413.